Thematic Mapper: Operational Activities and Sensor Performance at ESA/Earthnet

L. Fusco, U. Frei, and *A. Hsu*
Earthnet Programme Office—ESA/ESRIN, Frascati, 00044 Italy

ABSTRACT: The ESA-Earthnet Thematic Mapper image characterization performed in the framework of the LIDQA Program includes operational activities support, understanding of the instrument reference characterization and performance in time, and comparison of TM products generated by different processing systems. The paper overviews the different topics within the Earthnet Programme investigations.

INTRODUCTION

IN THE FRAMEWORK of the Landsat operational activities performed by the European Space Agency, Earthnet Programme Office (ESA-Earthnet) proposed to participate to the Landsat Image Data Quality Analysis (LIDQA) Program to evaluate the Landsat-4 and Landsat-5 system performances with emphasis on the Thematic Mapper. Both Earthnet Landsat stations of Fucino (Italy) and Kiruna (Sweden) have been equipped with new ground acquisition and processing equipment for this improved instrument. A third TM processing chain was also set up at the Earthnet Programme Office located at Frascati (Rome, Italy) as a Quality Assessment and Algorithm Development Facility to operate off-production quality assessment functions, and to develop and test new processing algorithms. All three systems are based on a Perkin Elmer 3252 mainframe, interfaced with an Array Processor FPS 120B, High Density Tape Recorder(s) 42 tracks ENERTEC-Schlumberger with high speed data synchronization/decommutation equipment, an I2S Image Display terminal and standard peripherals (Fusco, 1984). TM data acquisition started with Landsat-4 at Fucino in November 1982, and recording resumed with Landsat-5 at both stations in April 1984 after the X-band anomaly in February 1983. The TM processing chains have been operated experimentally since February 1983 for Landsat-4 and since June 1984 for Landsat-5, and have been operational since September 1984.

This paper reports on different aspects associated with the Thematic Mapper data. First, we summarize the operational experience gained so far from the acquisition, processing, and quality control standpoint. Second, we review the activities developed at Earthnet to access radiometric and geometric characteristics of the Thematic Mapper instrument. Then, the analysis of a temporal sequence of TM data acquired on the same geographic area is addressed. At last, we describe the experiment of comparing two sets of data acquired and processed by Earthnet and by NASA/NOAA, in particular an image acquired at the same time directly by Fucino and via Tracking and Data Relay Satellite (TDRS) by the National Oceanic and Atmospheric Administration (NOAA). In all investigations we devote our effort to the analysis of only the six reflective bands.

TM OPERATIONAL ACTIVITIES REPORT

ACQUISITION

Landsat-4 Thematic Mapper images have been acquired only at Fucino ground station. Of the total acquisition, about 500 scenes are cloud free (mainly on North Africa). Landsat-5 images have been acquired since 6 April 1984 at both Fucino and Kiruna. To optimize the job operated by the two stations, normally they divide their acquisition responsibility in the overlapped coverage area. Figure 1 indicates the total number of cloud-free scenes acquired over Europe by Fucino in 1984 (from 6 April to 31 December) from Landsat-5. All acquired data are kept in the Earthnet archive in raw acquisition format on High density digital tape (HDDT).

PROCESSING

TM data are processed by Earthnet upon user requests. Full and quarter scenes are produced either at 6250 or 1600 bpi tape density in either band sequential or band interleaved by line or single band format. Although various combinations of radiometric (e.g., raw, preflight, absolute, relative) and geometric (e.g., raw, without Payload Correction Data-PCD, with PCD) corrections are possible in the Earthnet processing scheme, to date the stan-

PHOTOGRAMMETRIC ENGINEERING AND REMOTE SENSING,
Vol. 51, No. 9, September 1985, pp. 1299-1314.

0099-1112/85/5109-1299$02.25/0

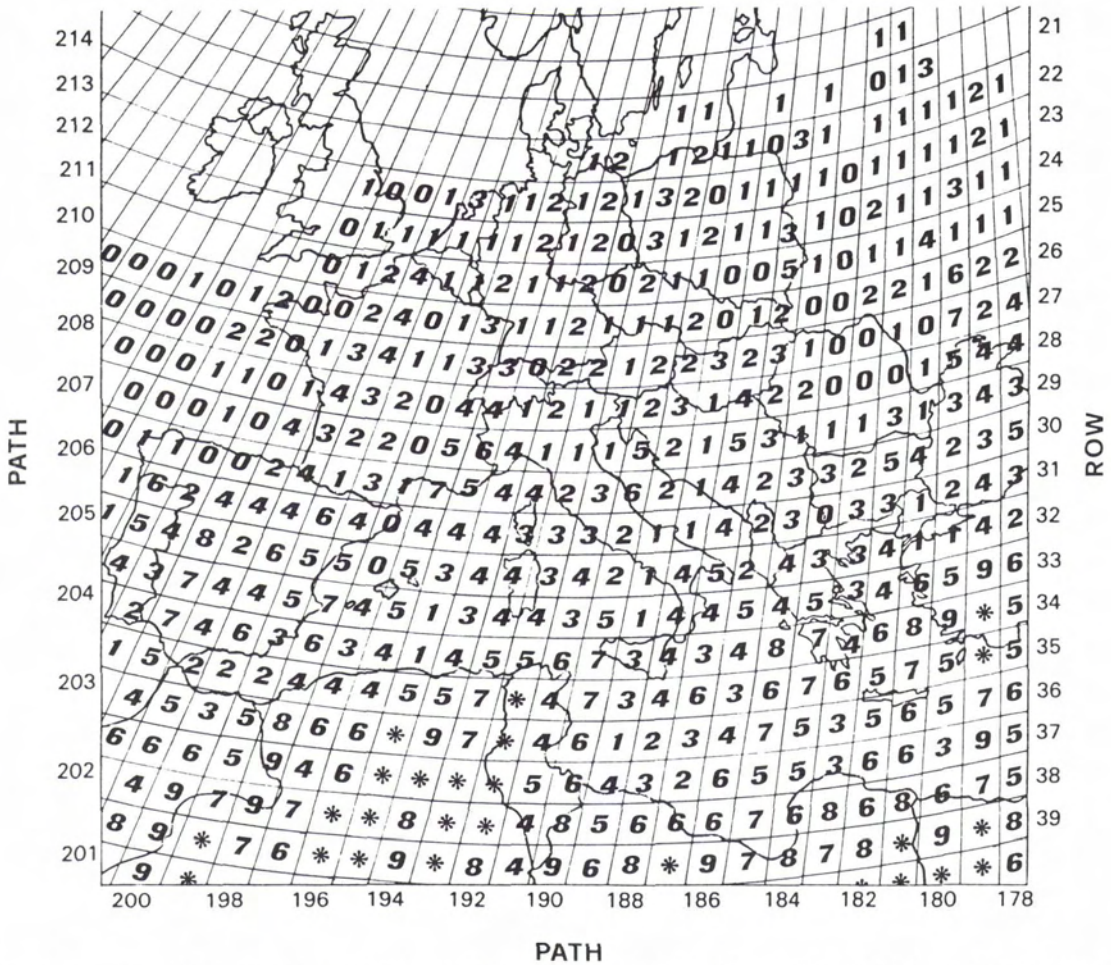

FIG. 1. Number of TM cloud-free frames acquired by Fucino (Italy) station in 1984 (6 April–31 December), from Landsat-5 over part of its coverage area. The numbers are derived from the Earthnet computerized image catalogs. *Indicates 10 or more cloud-free scenes.

dard system corrected products have the following corrections and the indicated quality level:

- Radiometric corrections: preflight corrections using NASA defined Radmin, Radmax, gain and offset are applied (NASA, 1984). No relative corrections are applied. No distinction is made between forward and reverse scans.
- Geometric system corrections: mirror scan velocity profile, line length variation, earth rotation and curvature, panoramic distortion, satellite altitude, velocity and attitude are applied. The corrections use housekeeping and ephemeris data available in the video data and in the PCD data stream. If the PCD data are not available (as it was in the case for data before 27 January 1983) or they are not of good quality, then the production will be completed with warnings and the product will have degraded (nonstandard) quality.
- Remapping: no specific map projection is employed for the standard output product. Data are centered around the World Reference System (WRS) frame center, relocated in longitude to the actual subsatellite point. No ground control points are used for the standard system-corrected product.
- Pixel size and resampling: system-corrected products are resampled at 30 × 30 m by nearest neighbor interpolation scheme.
- Band to band registration: bands are registered at the best one-half pixel position.

All data used in the investigations described below are Earthnet standard products unless otherwise indicated.

Quality Control

During and after production, quality checks are made on the digital TM products at the acquisition and production stations. These checks include, typically:

- residual striping assessment,
- residual swath jitter measurements,

- tape data content inspection (saturated data, dropouts, minor/major frame loss, printout of the most relevant radiometric and geometric parameters from tape),
- visualization of the produced CCT images on an image display terminal.

For each TM band, the residual striping is assessed using the following procedure:

- Generate the processed image histogram for each detector, in the range 1–254. Counts 0 and 255 are not used in this analysis (they contain saturation values).
- Compute the mean and standard deviation of each individual detector m_d, s_d, ($d = 1, \ldots, 16$) and of the entire band histogram, m and s.
- Compute the gain a_d and offset b_d to equalize each detector histogram to the entire band histogram.

$$a_d = s/s_d \text{ and } b_d = m - a_d m_d$$

- Compute the DN counts C' and C'' nearest to the 5 percent and the 95 percent of the total number of pixels in the histogram.
- For each detector, estimate the residual striping at C' and C'' by:

$$D'_d = (a_d - 1)C' + b_d$$
$$D''_d = (a_d - 1)C'' + b_d$$

The absolute maximum value of D'_d and D''_d should be within a specified threshold. In the operational environment this threshold is set up to 1.5 counts.

The residual jitter in the geometrically corrected image is measured by the displacement between adjacent lines of two consecutive swaths (i.e., detector 16 of swath N and detector 1 of swath $N + 1$). The displacement is determined by locating the maximum of the correlation coefficient profile between the two adjacent lines using given quality and threshold criteria. This method has been used to assess geometric performances of the TM instrument (Fusco and Mehl, 1985).

Only those products which did not meet the quality control standards will be sent to the Frascati Quality Assessment Facility for further inspection. If the analysis shows that the low quality of products was not caused by the processing, then the requested data will be distributed to the user with a warning message, otherwise the product will be rejected. The following are some typical warnings given to users:

- Large portion of saturated data (band 5 on desert areas is very often saturated. We have also measured some 30 percent of the total number of pixels at count 255).
- High residual striping after preflight radiometric correction (see comments in the section on *Residual Striping Analysis*).
- Large visual bright-target-saturation-effects over sea areas.
- No PCD available (larger jitter across swaths can be seen in the image).

Typical reasons for rejecting products are:

- minor/major frame loss or dropouts visualised on the image,
- residual striping too high.

Data Distribution

Figure 2 shows the number of TM digital products distributed in the period from January 1984 to February 1985. For simplicity, the number of products indicated there is given in quarter frame units with the assumption that a full scene product is equivalent to 4 quarter frames and 1 single band product is equivalent to 1 quarter frame. The figures do not include the rejected products, the products used to generate films, and the products used for internal validation. Of the distributed products, about 10 percent are also analyzed at Frascati for a detailed quality control. The number of final rejects for the two months of January and February 1985 is also reported in Figure 2.

Planned Improvements for TM Data Processing

With the experience gained from both the operational processing and the LIDQA investigations, Earthnet plans to improve its processing system on radiometric and geometric aspects (Barker, 1985). These improvements include:

- Make available the calibration parameters measured during the shutter obscuration time as the "before DC restore," "after DC restore," and "calibration peak integration" values for each image line on the CCT products.
- Generate the histogram and calibration parameters separately for the forward and the reverse scans.

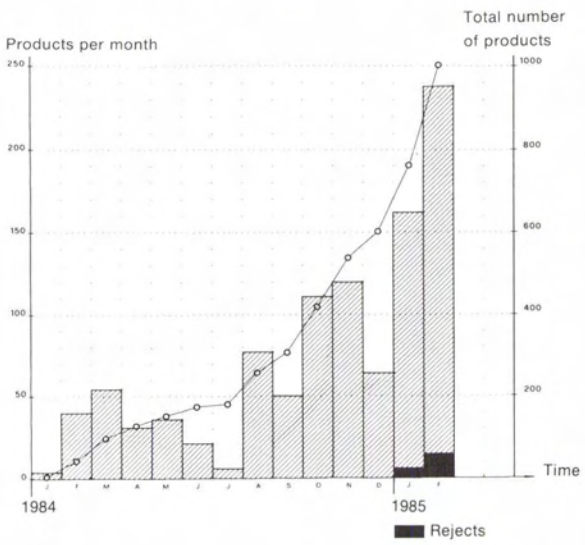

FIG. 2. Number of distributed TM CCT quarter frame equivalent products until February 1985. The figures do not include the products generated for internal validation or from which only photographic products were generated for distribution.

- Use the shutter obscuration calibration information in the absolute radiometric calibration processing.
- Generate and use an adequate model for the droop correction.

CHARACTERIZATION OF TM SENSOR: A REVIEW OF EPO ANALYSIS

The Earthnet Programme Office has conducted some studies on the radiometric and geometric characteristics of the TM sensor. Summaries of these studies are given here, and the full descriptions of these works are listed in the references.

Failed Detector Replacement on Landsat-4

The TM sensor of Landsat-4 has two failed detectors, detector 3 of band 5 and detector 4 of band 2. Various algorithms have been developed to replace radiances of the failed detectors (Bernstein *et al.*, 1984). We have implemented an optimal method for operational processing system. This method used the local relationship between the radiances of the two detectors next to the failed one and the radiances of the corresponding three detectors in a second band. The results are satisfying also in the case in which the second band is not strongly correlated (Fusco and Trevese, 1984 and 1985). Based on our experience it is suggested to use band 7 and band 3 to correct respectively the failed detectors in bands 5 and 2.

Radiometric Hysteresis

The name radiometric hysteresis is given to the within-line radiometric memory effect present in high contrasted areas even when the image is not saturated. The phenomenon appears evidently at the vicinity of sea and land in the first four bands. It has been shown in both Landsat-4 and Landsat-5. The results summarized here (Fusco and Trevese, unpublished paper, 1984) were achieved by processing subimages of the coast of Lebanon, path 174 row 38 (31 January 1983) Figures 3 and 4 and path 175 row 38 (8 May 1984). The following major considerations apply:

- In the representative case of band 4 for Landsat-4, across the sea/land transition, which takes place in some 10 pixels, the radiance increased from 10 DN on the sea to some 50 DN on the land. In this specific case the hysteresis effect lasts for approximately 300 pixels, reaching the absolute maximum value of about 0.7 DN at about 70 pixels from the transition and maintaining an asymptotic value of about 0.2 DN (this difference is explained by the droop effect).
- The amplitude of the net effect (maximum value minus droop effect) increases linearly with the radiance jump and is independent from the band within the first focal plane.
- No such effects have been detected in bands 5 and 7.

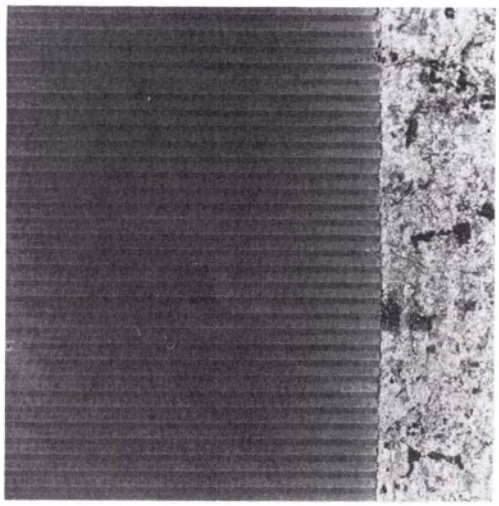

FIG. 3A. Subimage used for the radiometric hysteresis analysis (path 174, row 38, band 4—31 January 1983). The image has been contrast enhanced to emphasize the forward-reverse scan difference at the separation between sea and land.

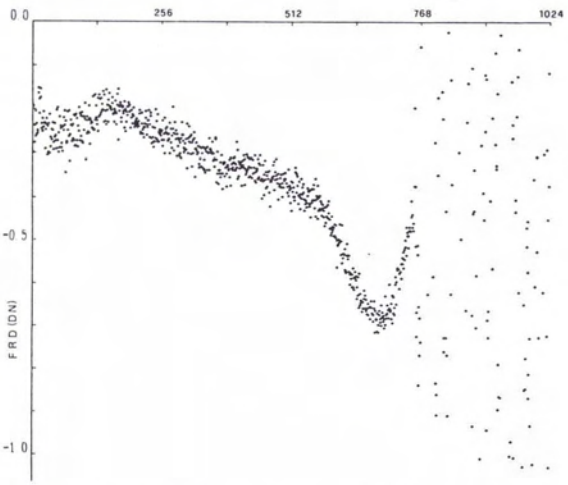

FIG. 3B. Forward minus reverse (FRD) scan average for the subimage in Fig. 3a at different pixel position. The absolute FRD max value is reached at about 70 pixels from the sea/land transition.

Our conclusion is that this phenomenon is very likely related to the bright target saturation and perhaps to the forward-reverse droop effect. Further analyses are in progress.

TM Line-to-Line Displacement Analysis using Correlation Techniques

A methodology to determine and analyze the displacement of adjacent TM lines (within the same

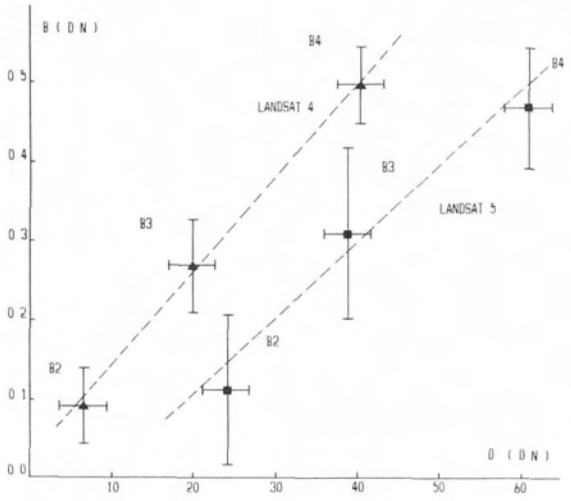

FIG. 4. Absolute value B (difference between the absolute max FRD value and the asymptotic value in Fig. 3b) versus the corresponding radiometric jump D (difference between average land DN and sea DN), for Landsat-4 and Landsat-5 and bands 2, 3, 4. The other band results are not plotted as they are not representative.

scan or not) has been implemented to perform the geometric characterization of the maximum of the correlation profile between the two analyzed lines (Fusco and Mehl, 1985). This methodology was used to characterize the within-scan geometry for both Landsat-4 and Landsat-5 in their early acquisitions. It has been reported that the main component of the across-scan jitter is a consequence of the regular variation of the scan length with a period of 7 scans. The method was also utilized to assess the band-to-band and within-band sensor to sensor across track displacement; the results are in agreement with NASA (1984).

MULTITEMPORAL ANALYSIS OF TM DATA

To evaluate the TM instrument and the performance of the Earthnet processing system over time, multitemporal studies of the same geographic area become necessary. These experiments include geometric accuracy analysis by means of ground control points (GCPs), frame center displacement, residual striping analysis and multitemporal comparison of GCP chips. For convenience, we selected the area around Rome, Italy, the second quadrant of path 191, row 31, as study area (Plate 1). Overall, 24 TM scenes as listed in Table 1 were analyzed and the results are presented.

GEOMETRIC ACCURACY ANALYSIS

The TM scene acquired on 11 July 1984 was selected as the reference image for the geometric accuracy analysis. The standard system corrected product was used to select GCPs. In total, 67 GCPs were identified together with their image coordinates obtained from the digital image display system and UTM map coordinates from 1:25,000 scale maps. This data set underwent an affine transformation analysis. The results (Figure 5) provide the following information:

- The average pixel size computed from the scale factor between maps and image in the along-track and in the cross-track directions are very close to 30 m (30.006 m and 30.002 m respectively),
- The RMS error for the 67 GCP is 20.45m,
- The rotation angle toward true North (from image to map) is 12.96°, which is different from the one (12.99°) computed by the orbital parameters.

We can conclude as follows:

- The Earthnet products are generated with a nearest neighbor interpolation algorithm, thus part of the residual errors should be attributed to this interpolation scheme.
- Although no map projection is applied to the Earthnet system corrected products, the residual errors are still maintained below one pixel. The results presented here are in agreement with those targeted by the design specifications and other Landsat investigators (Welch and Usery, 1984; Walker *et al.*, 1984).
- The plot of the error vectors (Figure 5) indicates residual errors are larger at the western part of the image, with a maximum error around 45 meters.

IMAGE FRAME CENTER DISPLACEMENT OVER TIME

A preliminary analysis of the frame center location over time was performed on the set of Rome images listed in Table 1. There are three sets of frame centers to compare:

- The WRS nominal frame center location is an a priori known position. For path 191 and row 31 the WRS Center is at 4627533 N and at 256475 E in UTM coordinates.
- The system computed frame center northing and easting position which is obtained during the system correction processing by: (1) computing the time the satellite passes at the WRS latitude using the best available mean orbital elements (predicted values), (2) extracting from the S/C PCD data stream of the orbital and attitude parameters required to compute the subsatellite point at the defined time, (3) computing the latitude, longitude, northing and easting location of the subsatellite point which will be then written on the CCT product in given records.
- The true frame center in northing and easting which is determined by transforming the GCP location on the images to maps.

As most of the images were partly cloud covered, a simplified procedure was taken to relocate GCPs on the different images. Considering that the computed north rotation angle is always within 0.1°, the

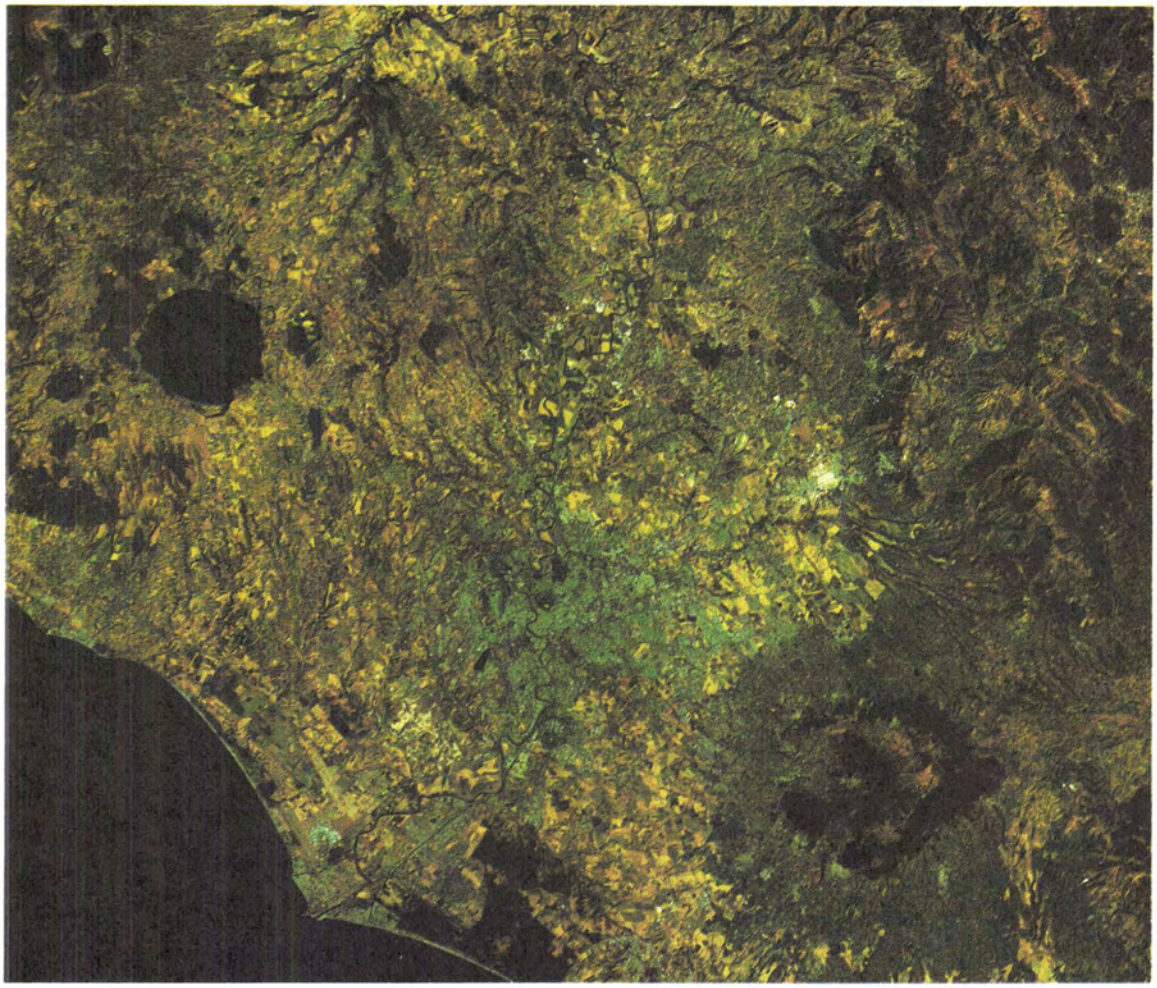

PLATE 1. The area of Rome (path 191, row 31) selected as reference image for the multitemporal analysis of TM data. This specific image product is especially made at 20 m resolution with cubic convolution interpolation in the band combination 5 red, 3 green, and 1 blue (original image in color).

major problem encountered in the relocation of the frame center with respect to the reference image is simply to find the offset. Therefore, only a few cloud-free ground control points, in some cases only one, were used to assess the offsets in respect to the reference images. In our analysis the WRS frame center location was compared respectively with the system computed and with the true frame centers. Table 2 summarizes the frame center parameters, and Figure 6 plots the easting of the true frame center in respect to the WRS values. It should be noted that:

- There is a systematic offset in both the northing and easting of the system-computed frame center in respect to the true frame center.
- When good information is available for processing these tested images, the standard deviations of northing and easting with respect to WRS are within 1.5 km and 2 km, respectively. The results can be indicators of the spacecraft performance.

In Figure 6 it must be noted the large excursion of the frame center longitude on the period of August to September 1984 which is set out of the specified 10 km maximum deviation expected by Landsat.

RESIDUAL STRIPING ANALYSIS

Landsat-5 scenes identified in Table 1 and processed with preflight radiometric correction were analyzed to assess residual striping with the method described in a previous section. Three classes of detectors are distinguished in each spectral band:

- Class 1 consists of detectors for which the mean of the detector histogram m_d is higher than one standard deviation s_{md} of the mean values for the band, i.e. for which: $m_d > m + s_{md}$.
- Class 2 consists of detectors for which: $m_d < m - s_{md}$.
- Class 3 consists of detectors for which m_d is closest to the total histogram mean m.

TABLE 1. LIST OF DIFFERENT SCENES (191/31/2) USED IN THE MULTITEMPORAL ANALYSIS

Ref. No.	Acq. Date	Miss.	Cyc.	Az.	El.	CC	Softw.	Remarks
1	5 DEC 82	4	9	155	22	70	7	no PCD
2	22 JAN 83	4	12	149	22	0	6	no PCD
3	7 FEB 83	4	13	147	26	80	7	
4	6 APR 84	5	3	136	47	40	8	
5	24 MAY 84	5	6	125	59	60	9	
6	9 JUN 84	5	7	121	60	40	6	
7	25 JUN 84	5	8	119	60	20	6	
8	11 JUL 84	5	9	120	59	0	6	
9	27 JUL 84	5	10	124	57	10	8	
10	12 AUG 84	5	11	129	54	30	7	
11	28 AUG 84	5	12	135	50	50	7	
12	13 SEP 84	5	13	141	45	0	7	
13	29 SEP 84	5	14	147	40	80	7	no PCD
14	15 OCT 84	5	15	151	35	0	7	
15	31 OCT 84	5	16	154	30	10	7	no PCD
16	2 DEC 84	5	18	156	22	80	7	
17	18 DEC 84	5	19	154	20	30	7	
18	19 JAN 85	5	21	150	22	60	7	
19	4 FEB 85	5	22	147	26	70	9	
20	20 FEB 85	5	23	145	30	10	9	
21	8 MAR 85	5	24	142	36	90	9	no PCD
22	24 MAR 85	5	25	140	42	70	9	
23	9 APR 85	5	26	137	48	90	9	
24	25 APR 85	5	27	133	53	70	9	

Legend:
- Ref. No. : Reference number as used in the paper and figures
- Acq. Date : Acquisition date
- Miss. : Landsat mission number
- Cyc. : Cycle in the mission
- Az. : Sun azimuth at frame center
- El. : Sun elevation at frame center
- CC : Cloud Cover in the quadrant in %
- Softw. : Processing software release number

The three classes are indicated in Figure 7 respectively by the symbols +, −, and *.

From Figure 7 we notice that for a few detectors in each band the preflight calibration may not be appropriate as a large residual striping is constantly present in the corrected image. The following is a list of detectors which could be assigned as class 1 or 2 for more than 70 percent of cases:

- band 1: detectors 2 and 1 overcorrected and 8 undercorrected
- band 2: detectors 6 and 8 overcorrected
- band 3: detector 2 overcorrected
- band 4: detector 1 overcorrected
- band 5: detectors 5 and 8 overcorrected and detectors 4, 7, and 11 undercorrected
- band 7: detectors 4 and 5 overcorrected and detectors 10 and 12 undercorrected

Although the results described here have been derived only from the frame 191/31/2, our operational quality control activities provide consistent results, cumulated from daily work. This analysis suggests that some parameters of the calibration corrections could be modified to reduce these systematic deviations. Alternatively, the relative radiometric corrections must be applied in all cases if the preflight calibration corrections remain unchanged.

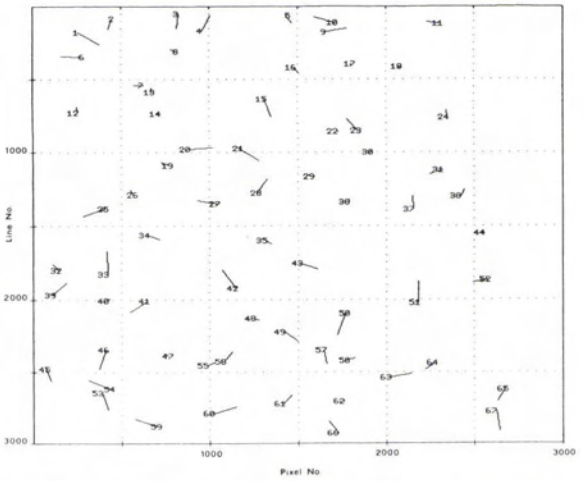

FIG. 5. Residual error plot in image space for reference image (11 July 1984). The number associated with each vector identifies the corresponding GCP. The error vectors and the GCP location are not mapped on the same scale.

ANALYSIS OF GCP CHIPS OVER TIME

To register images acquired at different times successfully one needs an adequate set of GCPs. However, the enhanced specifications and performances of the Thematic Mapper (narrow spectral bands, high spatial resolution, high radiometric sensitivity) represent some disadvantages for image registration since objects viewed at different times of the year show drastic changes in the radiometric responses. In general, the selection of the features to be used as GCP chips depends on such factors as the scale of reference maps, the pixel size of the image to be analyzed, the spectral response of the features, the season during which the image was taken, the size of the GCP chip, etc. The objective of the present analysis is to develop a method for identifying (1) the most suitable features and (2) the best spectral band or band combination to optimize the selection of GCPs for multitemporal analysis of Thematic Mapper data. In other words, we attempt to define a function which is able, given a TM image, to select the optimal subset of GCP and spectral band(s) to be used for the analysis of that specific image. The results given here are very preliminary. Among the 67 GCPs used for the geometric quality assessment of the Rome scene, three have been selected to illustrate the temporal behavior of three typical GCP features in different spectral bands: the first one labeled LAKE represents a portion of a lake; the second, FOREST, represents the edge of a forest; the third, BRIDGE, represents a highway over a river.

TABLE 2. SUMMARY OF FRAME CENTER PARAMETERS AS COMPUTED BY THE SYSTEM CORRECTION PROCESSING AND BY GCP RELOCATION OF THE FRAME CENTER

Ref. No.	Cy.	Easting Calc.	Easting True	North Angle	Orbit Incl.	S/C Altid.
1	9	257940	---	13.014	98.238	708465
2	12	256163	253790	13.019	98.231	707280
3	13	255925	252659	13.017	98.229	707520
4	3	257975	254264	13.030	98.250	708348
5	6	260658	257023	13.000	98.244	707965
6	7	258912	256106	13.013	98.243	707882
7	8	259392	256448	13.009	98.243	707433
8	9	261366	258446	12.992	98.242	707576
9	10	254852	251318	13.043	98.241	708287
10	11	*	245719	*	98.240	707863
11	12	*	241516	*	98.238	708292
12	13	*	245531	*	98.236	707562
13	14	252118	251363	13.057	98.235	707520
14	15	255128	258343	13.026	98.231	707780
15	16	261443	260203	12.977	98.232	707555
16	18	264976	258028	12.939	98.225	707818
17	19	263802	261124	12.947	98.223	707821
18	21	261342	258648	12.960	98.219	707530
19	22	259577	251854	12.970	98.215	707469
20	23	259120	250214	12.970	98.213	707557
21	24	260263	257300	12.955	98.208	707420
22	25	258935	249907	12.962	98.206	707717
23	26	259122	249230	12.958	98.204	707891
24	27	260905	257281	12.937	98.198	708143

* Data not available

Nominal Frame Center at: 256475 E
4627533 N

	Mean	Std. Dev.	
North Ang.	12.987	0.03681	deg.
Inclination	98.228	0.01550	deg.
Altitude	707782	292	m

Although typical GCP chip size is smaller, this analysis used a 63 × 63 pixel area, i.e., an area on ground of about 2 × 2 km. Among the 24 images indicated in Table 1, the three acquired on 22 January 1984, 11 July 1984, and 15 October 1984, respectively, were selected for this analysis. Plate 2 represents the chip BRIDGE for the three images (left to right) on the spectral bands 3, 4, and 5 (top to bottom). Two different functions have been considered: the first function used the OIF, Optimal Index Factor defined by Chavez *et al.* (1982) as

$$OIF = \sum_{i=1}^{3} SD_i / \sum_{j=1}^{3} |CC_j|$$

where SD_i are the standard deviations of three selected bands and CC_j are the correlation coefficients between the three possible pairs. In other words, the *OIF* says that the best band combination is made by those bands given the maximum sum of standard deviations and the minimum sum of correlation coefficients. As an example, we have selected the top four band combinations suggested by Colvocoresses (1984). We computed the *OIF* for each chip in each of these four combinations. For each band combination the best chip is the one which has the maximum sum of *OIF*s computed from images acquired at different time.

In a similar way, the best band combination is the one which maximises the sum of OIFs for the same chip computed from multitemporal images. Table 3a shows that the best chips are those of type LAKE or BRIDGE and the best band combinations are 1, 4, 5 and 3, 4, 5.

The second function is aimed to select the best single band for multitemporal GCP analysis. We have defined Band Optimal Index Factor,

$$OIF^B = \sum_{i=1}^{N} SD_i^B \cdot \sum_{j=1}^{N-1} |CC_j^B|$$

where SD_i^B are the standard deviations of the images in band B viewed at N different times, and CC_j^B are the chip correlation coefficients between the one chosen as a reference image and those taken at different times. In other words for a given chip the best band will be the one which has the largest standard deviations and correlation coefficients over time. As shown in Table 3b, reducing the choices to bands 3, 4, and 5, we conclude that the best bands are 5 and 4. In addition, the chips of FOREST type are the least successful chips for multitemporal analysis.

A further analysis has been performed on the 67 chips extracted from the Rome scene, using 20 different band combinations. Overall, for multitemporal chip analysis the best two band combinations are the 1, 4, 5 and the 3, 4, 5, and the best single band is band 4.

COMPARISON OF TM PRODUCTS FROM NASA/NOAA AND ESA-EARTHNET

The main objectives of the comparison of TM products generated by both ESA-Earthnet and NASA/NOAA operational processing systems have been (1) to identify the level of quality performance in the different operational correction systems and (2) to assess the compatibility of data exchange at different levels and in different formats. As the NASA/NOAA and ESA-Earthnet used different geometric correction schemes, the basic differences in image quality between these two agencies might lie in the geometric quality of their images. The major parameters for image production which may affect image geometry are listed below:

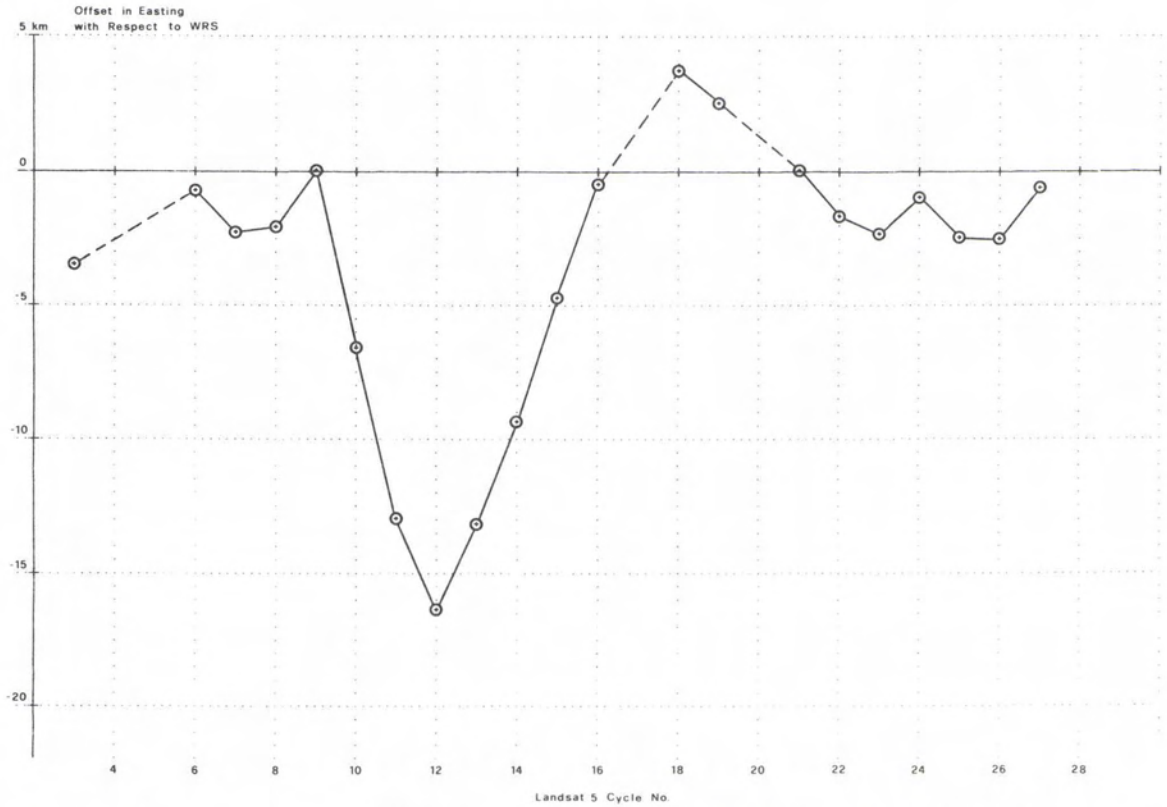

FIG. 6. True frame center easting in respect to reference WRS value at different Landsat cycle number. Note the large offset during cycle 11-13 (August–September 1984).

Parameter	NASA/NOAA	ESA-Earthnet
IFOV (after processing)	28.5 m	30 m
Resampling	Cubic convolution	Nearest neighbor
Map projection	SOM (preferred)	—
Scene correction data	32 kb/s	Embedded PCD
	Full orbit	Only scene data

No attempt is made here to describe in detail the hardware and software components of each system as they are described elsewhere (Fusco, 1984; Irons, 1985; Beyer, 1985). This report only describes two case studies: one is relative to the comparison of the first acquired Landsat-4 Detroit scene and the other of France.

In the first case study, the Detroit scene (path 16 and row 31) was acquired by Landsat-4 on 20 July 1982. Its NASA copy was processed with the ADDS/Scrounge system. The acquired raw data HDDT were transferred to the Kiruna station of Earthnet. There, data were transcribed on the standard Earthnet HDDT format and then processed by the Earthnet TM processing system. In this case study, 22 GCPs were determined using NASA LAS system on both NASA and ESA products. The image coordinates in scan line and pixel number and map coordinates in northing and easting of UTM projection measured from USGS 1:24,000 scale topographic maps were subjected to affine transformation analysis. The detail of this case study had been reported in Clark and Fusco (1984). The below summarized results represent the quality of fit between the image coordinates (lines and pixels) of NASA and ESA products and the corresponding UTM coordinates, i.e., NASA/USGS map and ESA/USGS map, respectively; and between the ESA product and the corresponding NASA image coordinates i.e., ESA/NASA.

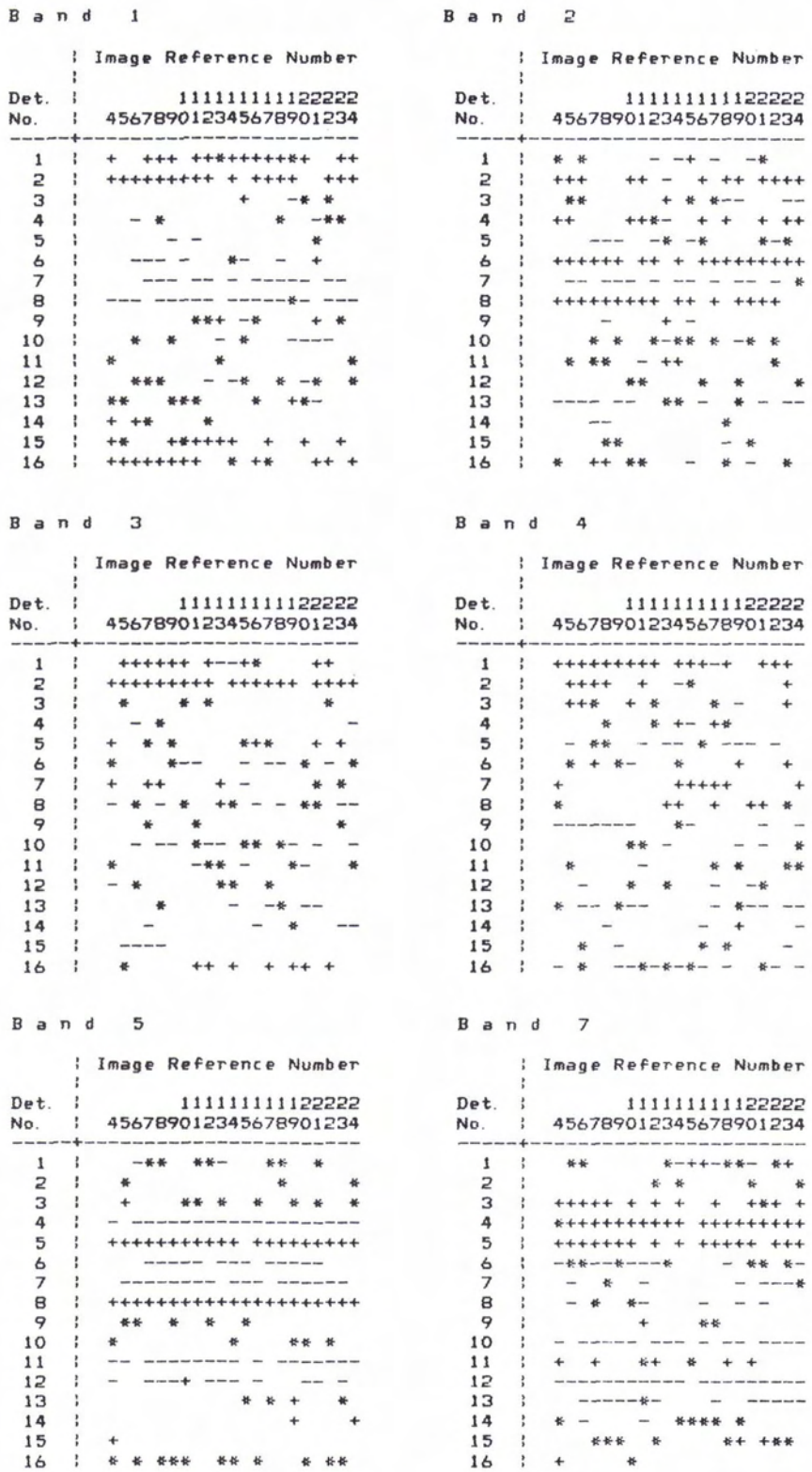

FIG. 7. Score of quality of preflight correction parameters.

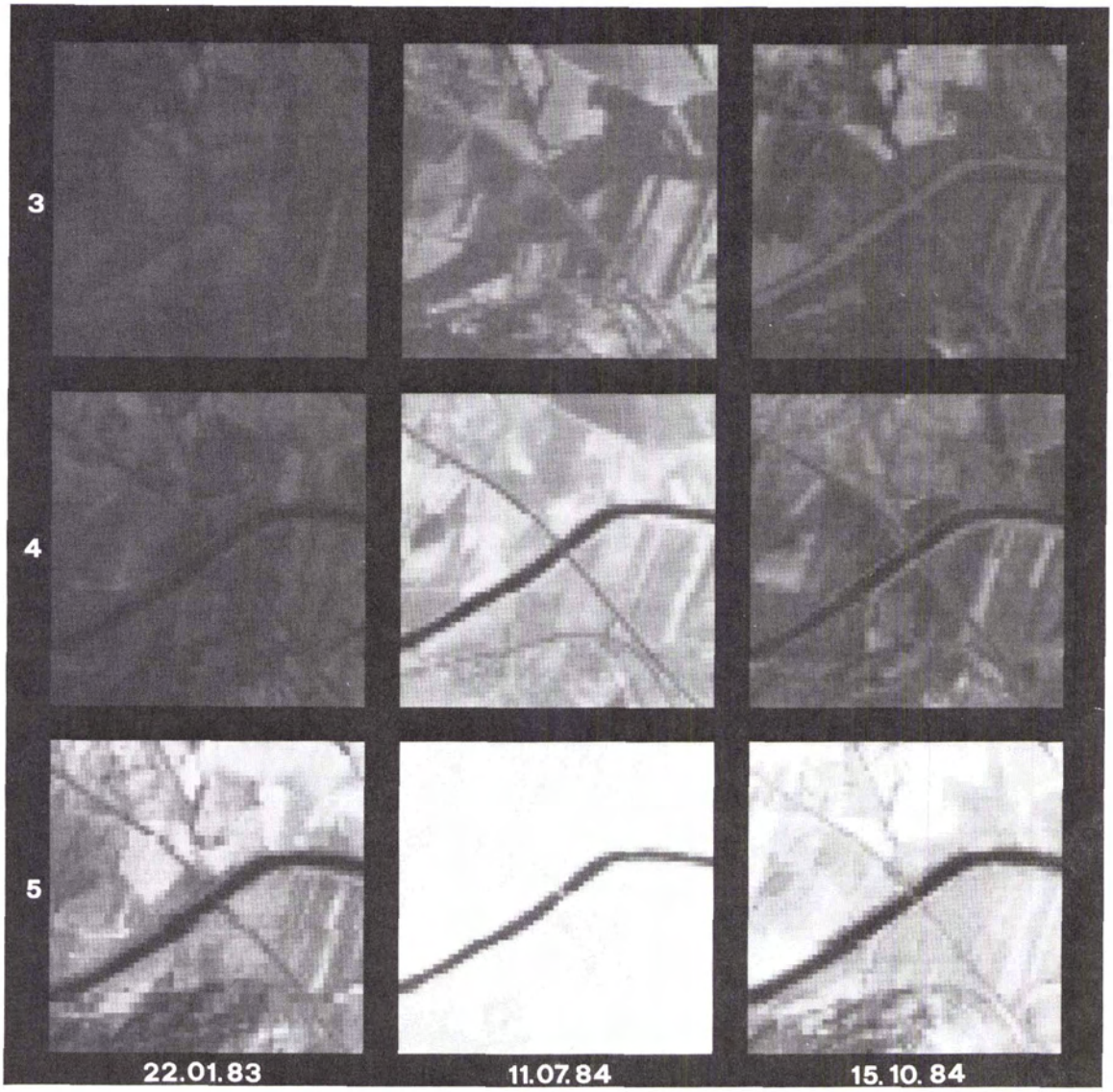

PLATE 2. The chip "BRIDGE" in three different bands from three different images. A fixed radiance scale is used for the images taken at different times.

	NASA/USGS Map	ESA/USGS Map	ESA/NASA
RMSE x (cross track)	18.34 m	22.24 m	27.30 m
RMSE y (along track)	22.81 m	25.89 m	18.11 m
RMSE x,y (vector)	29.27 m	34.13 m	32.70 m
Pixel Size in the Cross-Track Direction Computed by the Scale Factor of Affine Transformation	28.501 m	29.992 m	29.998 m
Pixel Size in the Along-Track Direction Computed by the Scale Factor of Affine Transformation	28.502 m	30.001 m	29.992 m
Rotation Angle	12.84°	12.50°	0.33°

TABLE 3A. SCORES FOR CHIP PERFORMANCE OVER TIME IN 3 BAND COMBINATION BASED ON OIF (CHAVEZ ET AL., 1982)

Chip	Ref. No.	Band Combination 1 4 5	2 4 5	3 4 5	1 4 7
Forest	2	12.292	10.358	11.240	10.460
	7	25.278	23.449	23.344	18.868
	13	19.850	17.030	22.026	17.591
	Total	57.420	50.837	56.610	46.919
Bridge	2	17.767	13.525	14.255	16.854
	7	47.833	48.132	49.204	38.637
	13	30.038	27.882	30.330	25.533
	Total	95.638	89.539	93.789	81.024
Lake	2	16.066	11.354	11.308	12.901
	7	47.967	33.415	36.483	35.736
	13	35.402	19.120	19.838	24.540
	Total	100.235	63.889	67.629	73.177

TABLE 3B. SCORES FOR CHIP PERFORMANCE OVER TIME FOR SINGLE BANDS

Chip		Band 3	Band 4	Band 5
Forest	SD^B	18.018	37.482	45.840
	CC^B	1.341	0.852	1.721
	OIF^B	24.162	31.935	78.271
Bridge	SD^B	28.535	39.127	63.660
	CC^B	0.898	0.910	1.718
	OIF^B	25.624	35.606	109.360
Lake	SD^B	17.259	74.825	69.854
	CC^B	1.958	2.527	2.658
	OIF^B	33.793	189.083	185.648

The overall results indicate that the products of NASA and ESA TM processing systems have good geometric quality. For example, the rotation angle between ESA's and NASA's products is 0.33°. Still, NASA's product is slightly better than ESA's. This may be attributed to the 28.5 pixel size and the cubic convolution resampling technique of NASA's processing system. However, the tendency of RMSE in the along-track direction to be larger than in the cross-track direction exists in both products. The second scene we selected for the case study is located at path 197, row 29, corresponding to the southern part of France. The image data were acquired by Earthnet Fucino station from Landsat-5 on 5 July 1984 and were processed by the Earthnet TM processing system. The same data were also acquired by NASA via TDRS and processed by NOAA using TIPS.

Because the large-scale topographic maps of southern France were not available to us, we could only perform an image to image comparison between NASA and ESA products. Thus, in the second case study, 85 tie points which could be identified in both ESA system-corrected full scene and in the four NOAA system-corrected quadrants processed by TIPS were selected and their coordinates in scan line and pixel number were obtained from the digital image display system. Again, we employed an affine transformation to assess the geometric quality of ESA products with respect to NASA's. First, the affine transformation was applied to analyze tie points located in each individual quadrant of NASA's product and in the corresponding part of ESA's full scene, separately, and then to the entire set of tie points of NASA's quadrants and ESA's full scene.

The results of these affine transformation analyses indicate an interesting situation which we have not encountered in our previous work. First, quadrants 2 and 4 have overall RMSE values greater than those in quadrants 1 and 3 in the along-track and cross-track directions and in error vectors (Table 4). No matter whether these overall values are computed from a single quadrant or are extracted from the full scene analysis, this difference exists. If we plotted these errors in an ordinary coordinate system with respect to zero mean (Figure 8a) then these plots show that a great number of tie points in quadrant 1 have positive residuals in the along-track direction and many tie points of quadrant 2 have negative residuals in the same direction. However, this situation is reversed in quadrants 3 and 4, more negative residuals in the along-track direction in quadrant 3 and more positive residuals in quadrant 4. The entire situation can be better presented by the error vector plot (Figure 8b). We can see that error vectors increase their values toward four corners and show a systematic pattern.

Since we are confident about the geometric quality of our products, with respect to the UTM projection, we would relate this systematic error situation to the SOM projection that NASA used to produce TM data (Walker, 1984). Maybe a second

TABLE 4. GEOMETRIC QUALITY OF ESA-EARTHNET PRODUCT WITH RESPECT TO NOAA/TIPS PRODUCT FOR SCENE 197/29 OF 5 JULY 1984

	Full Scene	Quad. 1	Quad. 2	Quad. 3	Quad. 4
No. of Tie Points	85	19	23	21	22
RMSE (Cross Track)	14.12 m	10.48 m	12.58 m	11.34 m	13.65 m
		(13.82 m)	(14.63 m)	(14.61 m)	(14.34 m)
RMSE (Along Track)	22.48 m	14.50 m	15.64 m	11.80 m	13.22 m
		(24.62 m)	(22.70 m)	(21.18 m)	(23.11 m)
RMSE (Vector)	25.22 m	17.00 m	19.06 m	15.51 m	18.08 m
		(26.85 m)	(25.62 m)	(24.50 m)	(25.84 m)
Pixel Size in the Cross Track Direction Computed by the Scale Factor of Affine Transformation	29.984 m	29.975 m	29.992 m	29.976 m	29.988 m
Pixel Size in the Along Track Direction Computed by the Scale Factor of Affine Transformation	30.006 m	29.994 m	30.012 m	29.996 m	30.016 m
Rotation Angle	< 0.05	< 0.03	< 0.03	< 0.07	< 0.07

NOTE: 1. All values in meters in this table are converted from pixel values by multiplying 28.5, assume NASA's product is accurate.

2. Values in parentheses indicate residuals of each quadrant in the full scene analysis.

or higher degree polynomial which can compensate larger errors in the corners of the scene would improve the closeness of fit between the image coordinates of the SOM projection and the unprojected products.

With regard to our second objective of this section, we found data exchange in the HDDT level was quite difficult because different types of tape recorders are used in NOAA and in Earthnet receiving stations. For all cases we had tested on the exchange of data in the HDDT level, the Detroit scene was the only case that data could be transcribed onto the standard Earthnet HDDT format. For all other cases the synchronization in reading the transcribed tape became incompatible (Clark and Fusco, 1984).

CONCLUSIONS

TM represents the best available spacecraft instrument for remote sensing application given the announced specification and the very stable performances as we can also derive from different images, processed in different ways by different agencies.

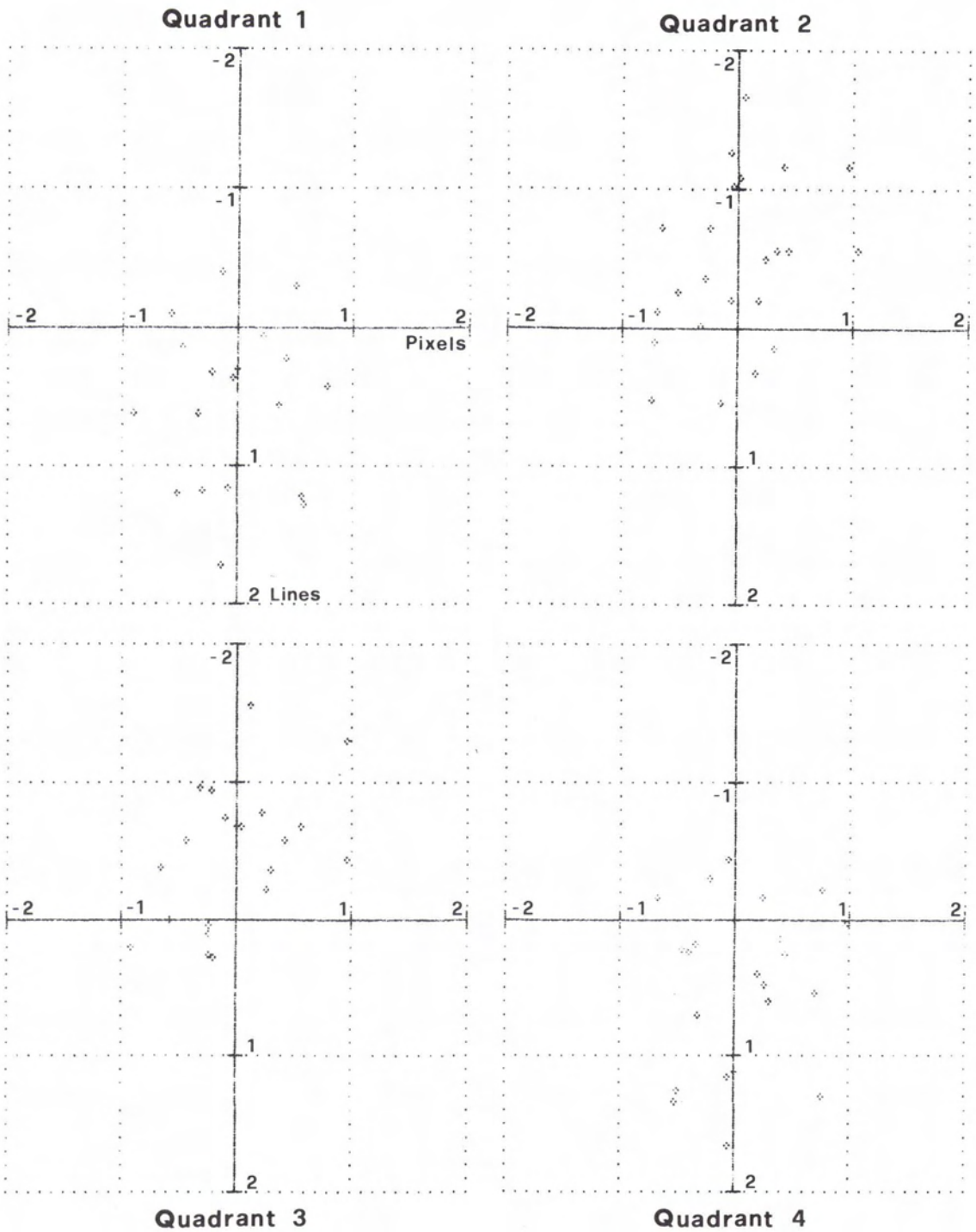

FIG. 8A. Distribution of error vectors for each quadrant in ESA-Earthnet versus NOAA/TIPS comparison (track 197, row 29—5 July 1984). Note: the plot reports the errors in pixel and line directions (line increases from top to bottom).

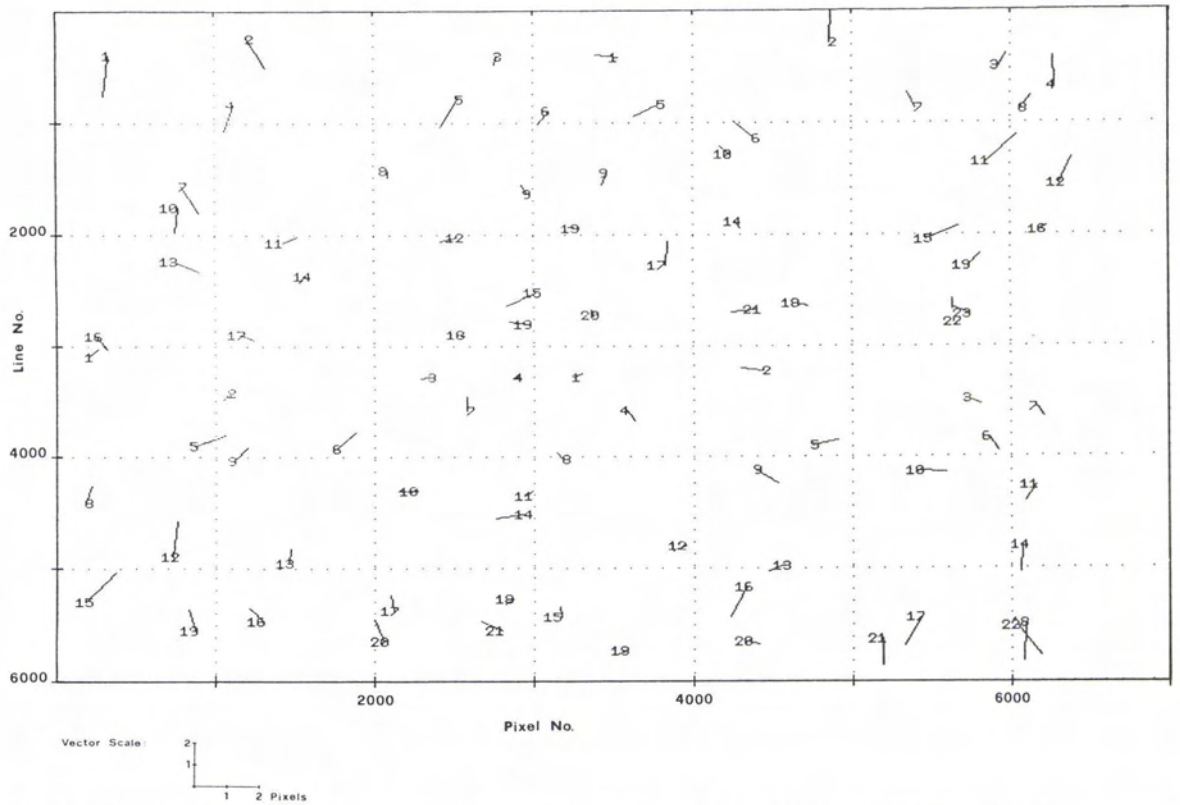

FIG. 8B. Error vector plots for the full scene product comparison of the ESA-Earthnet versus NOAA/TIPS (scene 197/29—5 July 1984)

According to analysis presented in this paper, we can conclude:

- The TM images were found of very good geometric quality as indicated by the small RMS errors from the 67 GCPs of Rome scene (20.45 m). The good geometric quality was also shown when registering ESA's products to NASA's at the same geographic area.
- The residual striping analysis showed a few detectors in every reflective band have preflight calibration bias, which need to be modified to compensate for these deviations.
- The within-scan variability of the type radiometric hysteresis is detectable in sea/land separation and it seems related to both bright target saturation and droop effect.
- During the first year of Landsat-5 life the spacecraft has been kept always in the specified orbit parameters except for the period August-September 1984.

Overall the Earthnet Programme Office has gained some experience by participating in the LIDQA Program, and these experiences will be used for improving product generation procedures.

REFERENCES

Arets, J., Berg, A., Fusco, L., and Gregoire, R., 1984. Earthnet MSS data supports CEC hunger-relief projects in the Sahel: *ESA Bulletin*, no. 40, pp. 66-71.

Barker, J. L., 1985. Relative radiometric calibration of Landsat TM reflective bands: NASA Conference Publication 2355, v. 3, pp. 1-219.

Bernstein, R., *et al.*, 1984. Analysis and processing of LANDSAT-4 sensor data using advanced image processing techniques and technologies: *IEEE Transactions on Geoscience and Remote Sensing*, v. GE-22, no. 3, pp. 281-288.

Beyer, E. P., 1985. An overview of the Thematic Mapper geometric correction system: NASA Conference Publication 2355, v. 2, pp. 87-145.

Chavez, P. S. Jr., Berlin, G. L., and Sowers, L. G., 1982. Statistical method for selecting Landsat MSS ratios: *Journal of Applied Photographic Engineering*, v. 8, no. 1, pp. 23-30.

Clark, B. P., and Fusco, L., 1984. Geometric comparison of Landsat Thematic Mapper data: an international experiment: *Proceedings of 6th LTWG Meeting*, June 12-15, 1984, NASA LIB-PRO-0014, Attachments pp. 17.1-17.21.

Colvocoresses, A. P., 1984. Mapping of Washington D.C.

and vicinity with the Landsat-4 Thematic Mapper: U.S. Geological Survey Miscellaneous Investigations Series, I-1616.

Fusco., L., 1984. Thematic Mapper: The ESA/EARTHNET ground segment and processing experience: *IEEE Transactions on Geoscience and Remote Sensing*, v. GE-22, no. 3, pp. 329-335.

Fusco, L., and Mehl, W., 1985. TM geometric performance: line-to-line displacement analysis (LLDA): NASA Conference Publication 2355, v. 3, pp. 359-388.

Fusco, L., and Trevese, D., 1984. TM failed detector data replacement: NASA Conference Publication 2326, v. 2, pp. 7-14.

——— 1985. On the reconstruction of lost data in images of more than one band: *International Journal of Remote Sensing*, v. 6 (in press).

Irons, J. R., 1985. An overview of Landsat-4 and the Thematic Mapper: NASA Conference Publication 2355, v. 2, pp. 15-46.

National Aeronautics and Space Administration 1984. Landsat to ground station interface description, Revision 8: GSFC 435-D-400.

Walker, R. E., *et al.*, 1984. An Analysis of LANDSAT-4 Thematic Mapper geometric properties: *IEEE Transactions on Geoscience and Remote Sensing*, v. GE-22, no. 3, pp. 288-293.

Welch, R., and Usery, E. L., 1984. Cartographic accuracy of LANDSAT-4 MSS and TM image data: *IEEE Transactions on Geoscience and Remote Sensing*, v. GE-22, no. 3, pp. 281-288.
